Geophys. J. R. astr. Soc. (1985) **80**, 695–713

Geomagnetic field analysis – III. Magnetic fields on the core–mantle boundary

David Gubbins and Jeremy Bloxham *Bullard Laboratories, Madingley Rise, Madingley Road, Cambridge CB3 0EZ*

Accepted 1984 September 18. Received 1984 September 18; in original form 1984 June 6

Summary. The method of stochastic inversion, previously applied to secular variation data, is applied to main field data. Adaptations to the method are required: non-linear, as well as linear, data are used; allowance is made for crustal components in the observatory data; and the prior information is specified differently. The requirement that the models should satisfy a finite lower bound on the Ohmic heating in the core provides strong prior information and gives finite error estimates at the core–mantle boundary.

The new method is applied to data from the epochs 1969.5 and 1980.0. The resulting field models are very much more complex than other models, such as the IGRF models extrapolated to the core, and show considerable small-scale detail which, on the basis of the error analysis, can be believed.

The flux integral over the northern hemisphere is computed at each epoch; the difference between the two epochs is approximately one standard deviation, suggesting that the question as to whether the decay of the dipole is consistent with the frozen-flux hypothesis has been resolved in favour of the hypothesis.

1 Introduction

Charts of the Earth's magnetic field are made periodically by various national agencies. This involves interpolation between measurements made in surveys, at permanent observatories, and nowadays from satellites. The usual method is to assume a potential field and to fit the coefficients of a truncated spherical harmonic expansion to the measurements by least squares. In this paper we aim to map the field at the core–mantle boundary (CMB), which requires somewhat different techniques.

We assume the Earth's mantle is an insulator and that the field is wholly of internal origin (except for a correction made to the *Magsat* data discussed in Section 3). The problem of calculating the core field becomes one of analytic continuation of the potential from the surface where measurements are made, at the Earth's surface or at satellite altitude some 500 km above, to the core surface. A surface measurement gives a weighted average of the core field, the weighting function being the appropriate Green's function for Laplace's

equation (Gubbins & Roberts 1983). It follows that we can only find an average of the core field rather than its value at a point; it also follows that short-wavelength core field will not be apparent in the observations because of the averaging process, and conversely any noise in the measurements will be amplified into the short-wavelength field, by the downward continuation process.

This instability that accompanies downward continuation is well known. Modern methods (for example Shure, Parker & Backus 1982) make use of uncertainties in the measurements to produce smooth core fields with as little short-wavelength component as possible. These methods cannot, however, reduce the errors in the core field that are dependent only upon the quality of the data and the extent of our prior information about the core field.

The first two papers of this series, Gubbins (1983, 1984, hereafter referred to as papers I and II) dealt with the analysis of secular variation. The difficulty with making point estimates on the CMB was side-stepped by dealing only with integrals over patches of the CMB bounded by field contours. The error in the field was assumed negligible compared with that in secular variation. In this paper we analyse the main magnetic field. Point estimates are required to define the contours used in previous work. We develop a technique that yields useful error estimates for the core field. It is based on the physical requirement that the dissipation associated with any allowed core field is finite.

There are several reasons why it is desirable to model main field (MF) rather than secular variation (SV). Most importantly we can make use of far more data: SV measurements are limited to permanent magnetic observatories whereas MF models incorporate satellite and survey data. A succession of MF models, all derived by a consistent method for various epochs, contains the information of not only the secular variation but also higher time derivatives.

There are two new problems that arise from MF analysis. The methods must be developed to cope with measurements, such as those of the total intensity, that depend non-linearly on the model. This requires an iterative solution and a fresh look at the statistical basis of the method, given in Section 2. Also the MF contains a significant short-wavelength crustal component which was eliminated from the SV data in papers I and II by using only those observatories that ran continuously throughout the period of investigation. This crustal field cannot be modelled by a core field and is effectively a source of noise in the data. Steps taken to reduce the effects of the crustal field are described in Section 3.

2 Method

2.1 NON-LINEAR DATA

The use of measurements of total or horizontal intensity, declination, or inclination, all require an iterative solution to obtain the model, necessitating some modifications to the basic method described in paper I. We take this opportunity to outline the Bayesian formulation of stochastic inversion. Jackson (1979) derives the stochastic inverse by two methods: first, he derives it using a minimum-variance estimation criterion; this was the formalism used in paper I of this series. However, as Tarantola & Valette (1982) have pointed out, the minimum-variance formalism is only applicable to linear problems – application of Jackson's form of the inverse to a local linearization of the problem is invalid. Tarantola & Valette derive the inverse using a method in which prior information is incorporated in terms of stochastic restrictions – the philosophy of Jackson's second derivation, the use of *a priori* data. For a complete account of this 'classical approach', as it is called, see Toutenburg (1982).

Here we describe the Bayesian formalism, detailed accounts of which are given by Box & Tiao (1973) and Bard (1974). We follow closely the development of Bard (1974). The Bayesian interpretation of probability is a mathematical expression of our degree of belief in some particular proposition, as opposed to the more restrictive frequentist interpretation in sampling theory. This enables us to represent our prior beliefs about the range of values taken by the coefficients in terms of a probability distribution which can be incorporated with the likelihood function (representing the information content of the data), using Bayes' theorem, to form the *posterior* distribution representing our *posterior* beliefs.

Using, wherever possible, the notation of Paper I, we write the model equation (the equations of condition) in the form

$$\boldsymbol{\gamma} = \mathbf{f}(\mathbf{m}) + \mathbf{e} \tag{1}$$

where $\boldsymbol{\gamma}$ is the D-dimensional data vector, $\mathbf{m}$ is the P-dimensional model vector of geomagnetic coefficients and $\mathbf{e}$ is the error vector. $\mathbf{f}$ is, in general, a non-linear functional of $\mathbf{m}$ and of the independent variables (r, θ, ϕ). In order to make P finite we truncate the spherical harmonic series at some degree L, where $P = L(L+2)$, with L chosen to be sufficiently high to ensure that the expansion has converged. In this way we have reduced the problem to one of parameter estimation without degrading the model specification in any way. We represent our prior beliefs about $\mathbf{m}$ in terms of the prior probability distribution $p_0(\mathbf{m})$ given by:

$$p_0(\mathbf{m}) = (2\pi)^{-P/2} \det{}^{-1/2} \mathbf{C}_m \exp(-\tfrac{1}{2}\mathbf{m}^{\mathrm{T}} \mathbf{C}_m^{-1} \mathbf{m}). \tag{2}$$

Equation (2) may be written:

$$\mathbf{m} \sim N_P(\mathbf{0}, \mathbf{C}_m) \tag{3}$$

meaning $\mathbf{m}$ is P-dimensional normally distributed with zero mean and covariance matrix $\mathbf{C}_m$. The choice of $\mathbf{C}_m$ will be discussed in the next section.

The information about $\mathbf{m}$ contained in the data $\boldsymbol{\gamma}$ may be expressed in a similar form. We assume

$$e \sim N_D(\mathbf{0}, \mathbf{C}_e) \tag{4}$$

where $\mathbf{C}_e$ is the covariance matrix of the measurement errors, assumed diagonal.

Then $\boldsymbol{\gamma}$ is a sample from the distribution $p(\boldsymbol{\gamma} : \mathbf{m})$ given by

$$p(\boldsymbol{\gamma} : \mathbf{m}) = (2\pi)^{-D/2} \det{}^{-1/2} \mathbf{C}_e \exp\{-\tfrac{1}{2}[\boldsymbol{\gamma} - \mathbf{f}(\mathbf{m})]^{\mathrm{T}} \mathbf{C}_e^{-1} [\boldsymbol{\gamma} - \mathbf{f}(\mathbf{m})]\}. \tag{5}$$

The likelihood function $L(\mathbf{m})$ is obtained by considering $p(\boldsymbol{\gamma} : \mathbf{m})$ as a function of $\mathbf{m}$ with $\boldsymbol{\gamma}$ fixed.

The prior distribution and the likelihod function are combined using Bayes' theorem to form the posterior distribution $p(\mathbf{m})$ by

$$p(\mathbf{m}) = k\, p_0(\mathbf{m})\, L(\mathbf{m}) \tag{6}$$

where k is a normalizing constant.

$p(\mathbf{m})$ expresses our beliefs about $\mathbf{m}$ after considering both our prior beliefs and the additional information furnished by the observations. Two statistics of $p(\mathbf{m})$ are of particular interest: the mode $\hat{\mathbf{m}}$ of $p(\mathbf{m})$ is the value of $\mathbf{m}$ in which we place the strongest belief. We shall refer to $\hat{\mathbf{m}}$ as the estimate of $\mathbf{m}$. Secondly, we are interested in the covariance matrix $\mathbf{C}$ of $p(\mathbf{m})$, although for non-linear problems we must, as will be shown later, exercise caution in its interpretation.

Taking logarithms in (6) gives

$$\log p(\mathbf{m}) = \log L(\mathbf{m}) + \log p_0(\mathbf{m}) + \log k,$$

i.e.

$$\log p(\mathbf{m}) = -\tfrac{1}{2}[\boldsymbol{\gamma} - \mathbf{f}(\mathbf{m})]^{\mathrm{T}} \mathbf{C}_e^{-1} [\boldsymbol{\gamma} - \mathbf{f}(\mathbf{m})] - \tfrac{1}{2}\mathbf{m}^{\mathrm{T}} \mathbf{C}_m^{-1} \mathbf{m} + (\text{constant terms}). \tag{7}$$

Seeking the mode of $p(\mathbf{m})$ is equivalent to maximizing $\log p(\mathbf{m})$, or equally to minimizing the objective function $\Phi(\mathbf{m})$ given by

$$\Phi(\mathbf{m}) = [\mathbf{\gamma} - \mathbf{f}(\mathbf{m})]^{\mathrm{T}} \mathsf{C}_e^{-1} [\mathbf{\gamma} - \mathbf{f}(\mathbf{m})] + \mathbf{m}^{\mathrm{T}} \mathsf{C}_m^{-1} \mathbf{m}. \tag{8}$$

The problem is reduced to one of non-linear optimization. Note that in deriving (8) no linearizing approximation has been made. Many algorithms exist for seeking the minimum of Φ (see Luenberger 1969 for details). Gauss's method yields the algorithm:

$$\mathbf{m}_{i+1} = \mathbf{m}_i + (\mathsf{A}_i^{\mathrm{T}} \mathsf{C}_e^{-1} \mathsf{A}_i + \mathsf{C}_m^{-1})^{-1} \{\mathsf{A}_i^{\mathrm{T}} \mathsf{C}_e^{-1} [\mathbf{\gamma} - \mathbf{f}(\mathbf{m}_i)] - \mathsf{C}_m^{-1} \mathbf{m}_i\} \tag{9}$$

where $\mathbf{m}_i$ is the model vector at the ith iteration

and

$$\mathsf{A}_i = \left. \frac{\partial \mathbf{f}}{\partial \mathbf{m}} \right|_{\mathbf{m} = \mathbf{m}_i} \tag{10}$$

is the Fréchet derivative at $\mathbf{m}_i$.

The procedure is terminated when

$$|\Phi(\mathbf{m}_n) - \Phi(\mathbf{m}_{n-1})| < \epsilon \qquad \text{where } \epsilon \text{ is small} \tag{11}$$

and the approximation

$$\hat{\mathbf{m}} = \mathbf{m}_n \tag{12}$$

assumed.

In the neighbourhood of $\hat{\mathbf{m}}$, we can expand $\log p(\mathbf{m})$ in a Taylor series (Bard 1974):

$$\log p(\mathbf{m}) \simeq \log p(\hat{\mathbf{m}}) - \tfrac{1}{2}(\mathbf{m} - \hat{\mathbf{m}})^{\mathrm{T}} \mathsf{H}^{-1} (\mathbf{m} - \hat{\mathbf{m}}) \tag{13}$$

where

$$\mathsf{H} = \left. \frac{\partial^2 \Phi}{\partial \mathbf{m}^2} \right|_{\mathbf{m} = \hat{\mathbf{m}}} \tag{14}$$

is the Hessian matrix.

Now,

$$\frac{\partial^2 \Phi}{\partial \mathbf{m}^2} = \frac{\partial}{\partial \mathbf{m}} \left\{ -2 \left(\frac{\partial \mathbf{f}}{\partial \mathbf{m}} \right)^{\mathrm{T}} \mathsf{C}_e^{-1} [\mathbf{\gamma} - \mathbf{f}(\mathbf{m})] \right\} + 2\mathsf{C}_m^{-1}$$

$$= 2(\mathsf{A}^{\mathrm{T}} \mathsf{C}_e^{-1} \mathsf{A} + \mathsf{C}_m^{-1}) - 2 \left(\frac{\partial^2 \mathbf{f}}{\partial \mathbf{m}^2} \right)^{\mathrm{T}} \mathsf{C}_e^{-1} [\mathbf{\gamma} - \mathbf{f}(\mathbf{m})]. \tag{15}$$

So, provided the expression

$$\left(\frac{\partial^2 \mathbf{f}}{\partial \mathbf{m}^2} \right)^{\mathrm{T}} \mathsf{C}_e^{-1} [\mathbf{\gamma} - \mathbf{f}(\mathbf{m})] \tag{16}$$

is small, then

$$\mathsf{H} \simeq 2(\mathsf{A}^{\mathrm{T}} \mathsf{C}_e^{-1} \mathsf{A} + \mathsf{C}_m^{-1}) \tag{17}$$

and $p(\mathbf{m})$ is approximately normal about $\hat{\mathbf{m}}$ with covariance matrix C given by

$$\mathsf{C} = (\mathsf{A}^{\mathrm{T}} \mathsf{C}_e^{-1} \mathsf{A} + \mathsf{C}_m^{-1})^{-1} \tag{18}$$

where the right sides of (17) and (18) are evaluated at $\hat{\mathbf{m}}$.

The condition (16) for this normality approximation to be valid requires that the

residuals are small compared with the extent around $\hat{\mathbf{m}}$ in which the neglect of second and higher derivatives is valid.

The practical implementation of this method differs slightly from that outlined above. As described in Paper I, we introduce a damping parameter λ so the objective function (8) becomes:

$$\Phi(\mathbf{m}) = [\boldsymbol{\gamma} - \mathbf{f}(\mathbf{m})]^{\mathrm{T}} \mathbf{C}_e^{-1} [\boldsymbol{\gamma} - \mathbf{f}(\mathbf{m})] + \lambda \mathbf{m}^{\mathrm{T}} \mathbf{C}_m^{-1} \mathbf{m}. \tag{19}$$

Large values of λ place more emphasis upon the prior information, while smaller values place more emphasis upon the fit to the data. The quadratic form $\mathbf{m}^{\mathrm{T}} \mathbf{C}_m^{-1} \mathbf{m}$ defines a norm of $\mathbf{m}$; hence, varying λ results in a trade-off between misfit and norm.

In practice, as also mentioned in paper I, we do not know $\mathbf{C}_e$ precisely. Instead, we know only the relative sizes of the elements of $\mathbf{C}_e$; in other words, we know $\mathbf{C}_0$ where

$$\mathbf{C}_e = \sigma^2 \mathbf{C}_0 \tag{20}$$

and σ^2 is an unknown scalar.

The algorithm (9) is unaltered upon substitution of the factor σ^2, since this factor is absorbed into the choice of λ. However, the covariance matrix (18) is affected: we must multiply $\mathbf{C}$ by the factor σ^2, so an estimator $\hat{\sigma}^2$ of σ^2 is required. An unbiased estimator is given by:

$$\hat{\sigma}^2 = \frac{[\boldsymbol{\gamma} - \mathbf{f}(\mathbf{m})]^{\mathrm{T}} \mathbf{C}_0^{-1} [\boldsymbol{\gamma} - \mathbf{f}(\mathbf{m})]}{D - \mathrm{tr}[(\mathbf{A}^{\mathrm{T}} \mathbf{C}_0^{-1} \mathbf{A})(\mathbf{A}^{\mathrm{T}} \mathbf{C}_0^{-1} \mathbf{A} + \lambda \mathbf{C}_m^{-1})^{-1}]} \tag{21}$$

so the covariance matrix $\mathbf{C}$ becomes

$$\mathbf{C} = \hat{\sigma}^2 (\mathbf{A}^{\mathrm{T}} \mathbf{C}_0^{-1} \mathbf{A} + \lambda \mathbf{C}_m^{-1})^{-1}. \tag{22}$$

The proof of (21) is accomplished by minor modification of the proof given, for a more general problem, by Theil (1963).

In Jackson (1979) and paper I, the concept of a resolution matrix was discussed. Here we define and interpet the resolution matrix in the same way, but with the same caveat attached as for the covariance matrix, that the residuals are within the linear range. The resolution matrix $\mathbf{R}$ is given by:

$$\mathbf{R} = (\mathbf{A}^{\mathrm{T}} \mathbf{C}_0^{-1} \mathbf{A} + \lambda \mathbf{C}_m^{-1})^{-1} (\mathbf{A}^{\mathrm{T}} \mathbf{C}_0^{-1} \mathbf{A}). \tag{23}$$

Note, (21) is equivalent to:

$$\hat{\sigma}^2 = \frac{[\boldsymbol{\gamma} - \mathbf{f}(\mathbf{m})]^{\mathrm{T}} \mathbf{C}_0^{-1} [\boldsymbol{\gamma} - \mathbf{f}(\mathbf{m})]}{D - \mathrm{tr}(\mathbf{R})}. \tag{24}$$

The trace of the resolution matrix $\mathrm{tr}(\mathbf{R})$ represents the effective number of degrees of freedom available for fitting the data. Typically D, the number of data, is 30 or more times larger than $\mathrm{tr}(\mathbf{R})$, so in (24) we approximate

$$\hat{\sigma}^2 \simeq \frac{1}{D} [\boldsymbol{\gamma} - \mathbf{f}(\mathbf{m})]^{\mathrm{T}} \mathbf{C}_0^{-1} [\boldsymbol{\gamma} - \mathbf{f}(\mathbf{m})] \tag{25}$$

the mean sum of squares of weighted residuals or 'misfit'.

2.2 PRIOR INFORMATION

Consider the estimate for the radial component of magnetic field at a point on the CMB. The variance of this estimate depends on the covariance matrix of the model parameters (geo-

magnetic coefficients). If the model parameters are uncorrelated the covariance matrix is diagonal. If the variances of the model estimates are independent of spherical harmonic order m, as they are for the spherically symmetric case, then the variance of a point estimate is

$$V_P = \sum_{l=1}^{\infty} (l+1)^2 (a/c)^{2l+4} v_l \tag{26}$$

(paper I, equation 10) where v_l is the variance of a geomagnetic coefficient of degree l, and a and c are the Earth and core radii.

The expression for V_P in (26) will converge only if v_l falls off sufficiently rapidly with increasing l. Specifically, it will converge if

$$v_l = o[(c/a)^{2l} l^{-3}] \tag{27}$$

because any series whose terms approach zero faster than l^{-1} is convergent. We will seek prior information in the form of a choice for v_l that is strong enough to make (26) converge. We could truncate the series at some degree L thus requiring v_l to be zero for $l > L$, but there is no physical justification for such a truncation. We could truncate the series when V_P reached some unacceptable level, but this would only have the effect of making V_P equal to the prescribed value – we would have assumed the answer!

Restricting the electrical heating associated with allowed fields does give sufficiently strong prior information for (26) to converge. The Ohmic heating in the core is given by

$$\Phi = \int_{\text{core}} \eta \frac{(\nabla \times \mathbf{B})^2}{\mu_0} \, dV \tag{28}$$

where η is the magnetic diffusivity.

Φ must not greatly exceed the heat flowing out of the Earth's surface, about 10^{13}W. Equation (28) is not useful because it involves the field throughout the core, whereas we only know its value at the core surface. A useful inequality from Gubbins (1975) is

$$\Phi > 4\pi\eta \sum_{l=1}^{\infty} \frac{(l+1)(2l+1)(2l+3)}{l} (a/c)^{2l+4} \sum_{m=0}^{l} (g_l^{m^2} + h_l^{m^2}). \tag{29}$$

Bounding the right side of (29) is a necessary, but not sufficient, condition that Φ itself be bounded; a necessary requirement is that

$$v_l = o[(c/a)^{2l} l^{-4}] \tag{30}$$

which makes the series for V_P converge faster than l^{-2}.

This constraint is still a very weak one because only the right side of (29) has been bounded, and this itself is only a lower bound on the true Ohmic heating. The Ohmic heating could be restricted further by truncating the series at some degree when the right side of (29) had reached some reasonable value, say 10^{13}W. For the calculations reported here this truncation level was so high as to make no difference to the point error estimates.

In paper II use was made of the frozen-flux approximation, in which dissipation is neglected, and secular variation models were calculated that satisfied the constraints exactly. Fitting the constraints involved projecting the model on to the constraints plane, a process that introduced short-wavelength components into the model. It is possible to fit any data by adding more and more short-wavelength field, but clearly a point will be reached when the energy in the short wavelengths becomes so great that the assumption of negligible diffusion is negated, and an inconsistency develops. This suggests a second choice of prior information in which the diffusion term entering the induction equation is restricted to some small value.

The radial component of the induction equation at the CMB is

$$\frac{\partial B_r}{\partial t} + \nabla_h \cdot (\mathbf{v} B_r) = (\mu_0 \sigma)^{-1} \left(\frac{\partial^2 B_r}{\partial r^2} + \frac{4}{r} \frac{\partial B_r}{\partial_r} + \frac{2B_r}{r^2} + \frac{\Delta B_r}{r^2} \right) \tag{31}$$

where ∇_h denotes the horizontal gradient, Δ is the angular part of $r^2 \nabla^2$ and $\mathbf{v}$ is the velocity of the core fluid. The radial gradients are discontinuous across the CMB so that the first two terms on the right side of (31) are unknown to us. The remaining terms on the right side can be calculated from surface data.

We will take the last two terms on the rhs of (31) as typical of the magnitude of the dissipation in the core. It will be an underestimate if there are strong radial field gradients in the boundary layer at the top of the core. Multiplying (31) by B_r and integrating over the core surface gives

$$\frac{d}{dt} \oint \tfrac{1}{2} B_r^2 dS + \oint B_r \nabla_h \cdot (\mathbf{v} B_r) dS = \eta \oint B_r \left(\frac{\partial^2 B_r}{\partial r^2} + \frac{4}{r} \frac{\partial B_r}{\partial r} \right) dS$$

$$+ \eta \oint B_r \left(\frac{2B_r}{r^2} + \frac{\Delta B_r}{r} \right) dS. \tag{32}$$

The first integral is representative of the strength of secular variation, the last of dissipation. For typical MF and SV models and $\eta = 1.6\,\mathrm{m^2\,s^{-1}}$, the latter is about 20 per cent of the former, which gives an indication of the validity of the frozen-flux approximation.

The dissipation integral can be expressed in terms of the geomagnetic coefficients as

$$\eta c^{-2} \sum_{l,m} (g_l^{m^2} + h_l^{m^2}) \, 4\pi \frac{(l+1)^2}{(2l+1)} [2 - l(l+1)] (a/c)^{2l+4}. \tag{33}$$

If we require that (33) converge for all fields, then we have prior information of the form

$$v_l = o[(c/a)^{2l} l^{-5}]. \tag{34}$$

This is a stronger requirement than (30) because of the extra factor of l. Unlike (30) the argument is not a rigorous one because it does not involve a proper bound.

2.3 ERROR ESTIMATES

Proceeding as in Paper I we calculate the model by truncating at some degree L that is sufficiently high to achieve numerical convergence. L is larger for MF calculations than it is for SV because there are more data and consequently more energy in the shorter wavelengths. As with SV the model converges before the error calculation, but by degree L the elements of the covariance matrix have converged on to a diagonal form with elements given by the prior information. The asymptotic forms can be used in estimating errors.

The variance of an estimate of the radial magnetic field at a point on the CMB is given by

$$V_P = \mathbf{a}^T \mathbf{C} \mathbf{a} \tag{35}$$

where the components of $\mathbf{a}$ have the form

$$(l+1)(a/c)^{l+2} P_l^m(\cos\theta) \begin{Bmatrix} \cos \\ \sin \end{Bmatrix} m\phi.$$

The contribution to V_P from terms up to degree L can be found from the calculated covariance matrix. Above degree L the asymptotic forms may be used fo find the 'remainder' variance $V_P^{(R)}$.

$$V_P^{(R)} = \sum_{l=L+1}^{\infty} v_l (a/c)^{2l+4} (l+1)^2 \tag{36}$$

where v_l can take one of two forms depending on whether (30) or (34) is used for the prior information.

In the case of (30) we take

$$v_l = \frac{\sigma^2}{4\pi\lambda} (c/a)^{2l} (2l+1)/l^5 \tag{37}$$

where σ^2 is the squared misfit and λ the damping constant. This form gives a series in (30) that decreases as l^{-1}. Thus while the norm (30) does not converge, the point variance is given by a series that converges as l^{-2}. The factor of 4π and the precise functional dependence on l are chosen to simplify the analysis. Equation (36) becomes

$$V_P^{(R)} = (a/c)^4 \sigma^2/4\pi\lambda \sum_{l=L+1}^{\infty} \frac{(l+1)^2 (2l+1)}{l^5} \tag{38}$$

$$\simeq (a/c)^4 \sigma^2/2\pi\lambda L.$$

In the case of (34) we take

$$v_l = \sigma^2/4\pi\lambda (c/a)^{2l} (2l+1)/l^6 \tag{39}$$

and (36) gives

$$V_P^{(R)} \simeq (a/c)^4 \sigma^2/4\pi\lambda L. \tag{40}$$

Equations (38) and (40) can be used to estimate the remainder variance once the damping constant has been chosen and the misfit calculated.

In practice we find that the core fields (models) are quite insensitive to the choice of prior information; only the errors depend on it in any significant way. The strength of prior information depends also on the damping constant. The physical arguments apply only to geomagnetic coefficients at very high degree, and so it is crucial that our data be good enough to resolve out to a high enough degree for the prior information to take over, otherwise the prior information will be too strong at intermediate degree, leading to optimistic error bounds. For the models reported in this paper, the prior information appears to take over at about degree 14, and harmonics of degree greater than 20 are effectively zero.

In contrast to the fields, the error bounds depend critically on the choice of prior information, particularly the contribution from high degree terms.

3 Data

3.1 1980 MODEL

This model was based on a selection of *Magsat* measurements made on quiet days at dawn. The data were selected to give equal area coverage, with one location for an area about $5^\circ \times 5^\circ$ at the equator. These data were supplied to us by Drs R. H. Estes and R. A. Langel of Goddard Space Flight Center. A correction was made for the external effects by subtracting the external field calculated by Langel & Estes (1984). This gave three component measurements at 1262 locations. Above about 50° magnetic latitude external effects become very large in the horizontal component. Only vertical component measurements were used at 392 locations at these latitudes; in total 4178 measurements were used. The locations were supplied in geocentric coordinates, and these were used in the calculations. Equal weights were assigned to all these data.

3.2 1969.5 MODEL

Most of the data on which this model was based are total field intensity observations from the *OGO-6* satellite which flew in a polar orbit. The *OGO-6* data used here were chosen from a set of magnetically quiet period data from 1969 and 1970, provided by Goddard Space Flight Center; further details of these data may be found in Langel, Coles & Mayhew (1980). The 4270 observations which we used have a mean epoch of 1969 August and were chosen to be approximately equal-area in distribution and with as large as possible an interval between successive data points along tracks.

Because total field intensity data give poor resolution of the sectorial harmonics in the spherical harmonic expansion, it was necessary to supplement the dataset with observatory annual means. Synthetic calculations showed that our observatory set was sufficient to resolve the sectorial harmonics satisfactorily. This point is discussed more fully in the Appendix. A problem inherent in the use of observatory data for modelling the core field is that these data contain a substantial component due to crustal magnetization, generally of about 300 nT. Allowance was made for the crustal component in one of three different ways:

3.2.1 Category A observatories

These observatories had records running from 1969.5 until at least 1976.5 with no apparent uncorrected changes in baseline. The crustal component was estimated as the difference between the observed values of the field at the last available epoch prior to 1980.0 and the values calculated from the model D80111 in Fig. 2, corrected, where necessary, for secular variation using IGRF80: model D80111 being taken as a good approximation to the core field at 1980.0.

3.2.2 Category B observatories

Observatories not in category A but for which a crustal correction, valid at 1969.5, is available from Langel, Estes & Mead (1982). The crustal corrections are shown in Table 1.

3.2.3 Category C observatories

All other observatories: for these no correction was possible.

3.2.4 Weighting of the data

OGO-6 data were all assigned a standard error of 6 nT. Category A and B observatories were assigned standard errors comprising two components: a component of 20 nT corresponding to errors in the crustal correction and a component representing observational errors estimated by the method described in Shure *et al.* (1983).

Category C observatories were assigned a standard error of 300 nT. The observatory distribution is shown in Fig. 1. All data were given in geodetic coordinates, and the model calculations were carried out with the usual ellipticity correction.

4 Results

4.1 MODELS FOR 1969.5 AND 1980.0

Two models are shown in Figs 2 and 3, using the second form of v_l (34), with damping constant $\lambda = 10^{-11}$. The weight matrix, C_0, was diagonal with weights given in Table 1. The

Table 1. Observatory crustal corrections and weights. Corrections in nT, weights in 0.1 nT.

OBSERVATORY	CRUSTAL CORRECTIONS			WEIGHTS		
	X	Y	Z	X	Y	Z
ALERT	7	39	-117	236	256	311
HEISS ISLAND	100	-680	1133	276	231	323
CHELYUSKIN	-49	-99	-46	228	205	293
THULE	-37	123	26	210	201	206
MOULD BAY	-16	-9	-54	206	231	221
RESOLUTE BAY	57	24	48	225	213	216
BEAR ISLAND	-92	57	14	200	201	206
DIKSON	-55	-128	-246	218	206	213
BARROW	-23	-63	-13	231	216	333
TROMSO	96	-400	119	213	201	213
GODHAVN	259	-227	488	206	203	221
ABISKO	-5	69	29	213	203	223
LOPARSKAYA	70	331	-552	208	221	211
SODANKYLA	-187	-97	-582	205	226	203
UELEN	-113	47	-58	216	233	233
COLLEGE	2	-57	-90	206	216	203
BAKER LAKE	135	-54	-87	201	210	256
LEIRVOGUR	-273	596	-485	210	226	233
DOMBAS	-86	-36	-265	206	216	201
YAKUTSK	54	-1226	116	205	216	240
PODKAMENNAYA TUNGU.	45	15	-294	201	201	203
NARSSARSSUAQ	-273	269	507	225	206	231
NURMIJARVI	267	-85	126	208	221	205
LERWICK	-134	182	26	205	230	205
STEKOLNI	-304	-747	34	201	201	211
VOEIKOVO	63	36	-233	208	225	216
LOVO	32	21	17	206	221	203
FORT CHURCHILL	-154	-11	-250	206	218	218
SITKA	0	-2	-81	208	218	203
VYSOKAYA DUBRAVA	-298	-112	-483	201	200	200
TOMSK	0	0	0	3000	3000	3000
RUDE SKOV	29	11	-44	206	221	203
KAZAN	-295	-316	-240	203	201	201
KRASNAYA PAKHRA	129	-11	244	205	221	213
ESKDALEMUIR	-7	-40	-62	206	216	206
GREAT WHALE	257	110	-55	223	205	245
KLYUCHI	165	-89	-17	205	200	205
MEANOOK	114	9	-120	210	233	231
HEL	50	-146	-79	200	201	206
PLESHCENITZI	279	193	-104	201	200	203
WINGST	51	60	-68	208	218	201
PETROPAVLOVSK	-357	225	272	201	201	201
WITTEVEEN	15	13	-81	210	216	206
PATRONY	12	46	-65	231	208	276
NIEMEGK	-38	14	-77	206	216	201
VALENTIA	109	-44	16	205	221	210
BELSK	109	151	314	205	218	201
HARTLAND	-57	13	58	206	218	206
DYMER	-9	97	133	203	208	203
MANHAY	0	0	0	3000	3000	3000
DOURBES	-3	-11	71	206	216	201
PRUHONICE	0	0	0	3000	3000	3000
LVOV	153	139	154	213	221	218
BEREZNIAKI	-424	15	339	211	213	243
BUDKOV	-52	-3	-32	211	203	206
VICTORIA	17	3	-311	206	210	211
WIEN	23	7	4	210	213	216
NEWPORT	-48	105	-139	203	203	203
FURSTENFELDBRUCK	-25	-2	-2	208	215	205
CHAMBON-LA-FORET	-92	-20	104	208	208	203
HURBANOVO	2	-9	-56	231	206	210
ULAN BATOR	-3	-56	-104	203	200	216
NAGYCENK	22	8	-46	213	206	283
ST JOHNS	34	20	6	201	203	203
REGENSBERG	-7	11	-46	206	203	201
YUZHNO SAKHAL	36	-166	-151	206	203	206
TIHANY	-27	18	-55	213	208	206
STEPANOVKA	-107	-690	59	201	201	211
OTTAWA	114	-147	156	201	201	201
SURLARI	2	-22	-80	221	213	231
GROCKA	-45	-17	-84	208	213	208
ROBURENT	0	0	0	3000	3000	3000
MEMAMBETSU	-254	140	67	225	203	218
GORNOTAYEZHNAYA	-26	-13	-65	245	213	270
ALMA ATA	125	36	-155	208	243	256
PANAGYURISHTE	-208	-160	-207	215	206	226
LOGRONO	-4	-3	38	211	211	203
L'AQUILA	-19	42	-17	208	210	208
DUSHETI	-236	16	-121	213	203	238
YANGI BAZAR	-304	53	-97	200	200	200
KANDILLI	181	131	-24	208	215	213
EBRO	15	-2	-34	206	213	203
COIMBRA	3	-9	20	223	213	218
BOULDER	-31	53	-176	215	201	218
PEKING	595	-226	469	268	210	236
TOLEDO	-4	4	2	213	206	203
MIZUSAWA	-103	47	-251	228	203	243
FREDERICKSBURG	39	-61	127	261	203	281

Table 1 – *continued*

OBSERVATORY	CRUSTAL CORRECTIONS			WEIGHTS		
	X	Y	Z	X	Y	Z
ASHKHABAD	142	105	55	218	206	235
SAN MIGUEL	592	468	1807	500	500	500
ALMERIA	-26	20	15	211	208	205
SAN FERNANDO	105	38	-96	228	231	498
KAKIOKA	-23	17	-97	201	200	200
TEHERAN	0	0	0	3000	3000	3000
KANOZAN	-72	40	-52	218	206	200
SIMOSATO	-58	42	-1	253	203	208
DALLAS	0	0	0	3000	3000	3000
TUCSON	-98	-64	124	213	203	218
KANOYA	-35	43	-44	261	201	203
ZO-SE	-271	71	231	300	206	206
DEHRA DUN	-15	-28	63	206	211	243
QUETTA	-16	78	-35	201	201	203
LHASA	0	0	0	3000	3000	3000
HELWAN	0	0	0	3000	3000	3000
TENERIFE	-447	105	-1042	241	215	776
LUNPING	-15	41	55	205	301	206
TAMANRASSET	35	-256	-42	201	200	200
CHA PA	-120	-91	-3	293	213	323
HONOLULU	-191	87	-335	208	201	203
TEOLOYUCAN	-124	3	-12	215	261	245
ALIBAG	-140	456	689	258	213	221
SAN JUAN	-70	184	176	200	200	201
HYDERABAD	290	15	455	208	300	255
M'BOUR	86	27	58	213	203	205
MUNTINLUPA	-73	-58	32	236	208	221
GUAM	109	86	67	220	205	206
ANNAMALAINAGAR	125	-91	-91	230	221	263
KODAIKANAL	-571	275	-62	226	300	231
ADDIS ABABA	494	-2	81	201	203	200
TRIVANDRUM	250	195	196	206	200	201
IBADAN	0	0	0	3000	3000	3000
PARAMARIBO	0	0	0	3000	3000	3000
FUQUENE	77	-68	63	201	203	311
BANGUI	-198	-13	244	206	236	206
MOCA	0	0	0	3000	3000	3000
TATUOCA	0	0	0	3000	3000	3000
NAIROBI	11	32	13	213	203	228
LWIRO	0	0	0	3000	3000	3000
BINZA	0	0	0	3000	3000	3000
TANGERANG	23	71	42	526	331	728
LUANDA BELAS	276	-20	217	215	203	270
PORT MORESBY	-15	36	266	205	208	220
HUANCAYO	55	50	41	228	201	256
APIA	-79	220	-885	213	210	203
TANANARIVE	372	0	-447	216	210	236
TSUMEB	12	-62	87	205	201	203
LA QUIACA	23	-1	54	238	251	205
VASSOURAS	39	-51	-33	216	203	203
MAPUTO	312	52	-127	218	203	213
PILAR	-13	0	1	231	233	206
GNANGARA	-22	-130	147	201	206	236
HERMANUS	1	18	23	218	201	201
TOOLANGI	18	-27	40	205	210	203
AMBERLEY	-44	-17	70	206	205	211
TRELEW	0	0	0	3000	3000	3000
PORT AUX FRANCAIS	191	206	656	206	231	326
MACQUARIE ISL.	244	-3	291	206	208	208
ARGENTINE ISL.	80	-71	483	200	200	201
MIRNY	-95	63	-447	206	208	283
DUMONT DURVILLE	-153	-405	-2860	248	253	413
MAWSON	37	33	165	213	221	323
MOLODEZHNAYA	20	-118	-283	233	213	555
SYOWA BASE	0	0	0	3000	3000	3000
SANAE	-45	-31	12	203	203	206
NOVOLAZAREVSKAYA	-273	92	36	208	221	451
SCOTT BASE	-2276	-937	-3767	215	215	228
VOSTOK	-20	148	14	286	245	273
MAURITIUS	H & Z USED: NO CORRECTIONS APPLIED					

misfits were $\sigma = 1.09$ and 1.29 respectively. The calculation was terminated at degree 20, which gave satisfactory numerical convergence. The traces of the resolution matrices were 155 and 150 respectively, indicating that both models had a similar balance of prior information and data.

The models show very much more detail than core fields based on the IGRF or DGRF for 1970, and more detail than *Magsat* models, such as model GFSC 9/80 of Langel *et al.* (1982), when truncated at low degree; they bear more resemblance to model GSFC 9/80 when truncated near degree 12. The advantage of this method is that we have error estimates and can therefore decide which aspects of the detailed structure can be believed.

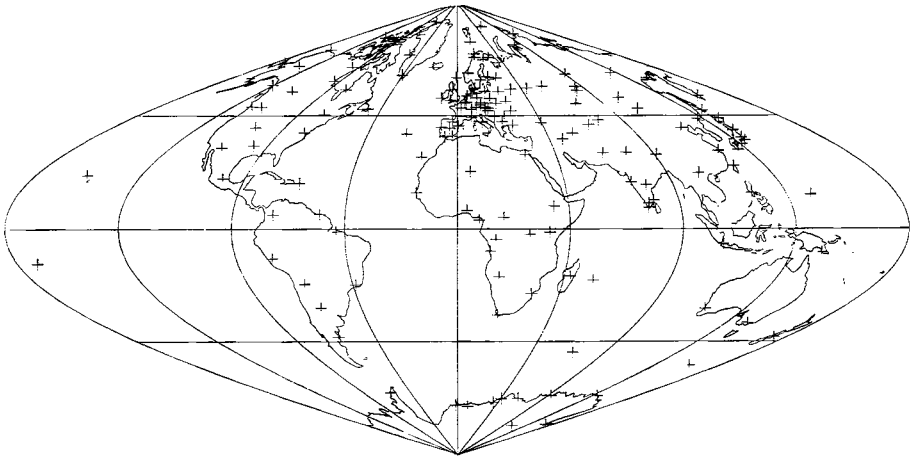

Figure 1. Observatories used for the 1969.5 field models plotted on a Sanson–Flamsteed projection.

Error estimates were calculated at 5° intervals over the entire core surface for each model using the covariance matrices. The remainder errors were 16 and 19 μT respectively. These were combined with each point variance based on the series up to degree 20 to give typical errors of 28 and 36 μT respectively. The contour intervals in Figs 2 and 3 are at an interval of 100 μT, so our error analysis indicates that the small-scale features are indeed well resolved.

The remainder errors are independent of position. The errors up to degree 20 are not uniform over the whole sphere, and for the 1980 model they vary from about 23.8 μT near the poles to 22.6 μT near the equator. This is because only vertical component measurements were used at high latitudes. For the 1969.5 model the errors to degree 20 are smallest near the poles (26 μT) and largest at the equator (33 μT), because of the preponderance of total field data. The variances of the sectorial harmonics, which are not well resolved by the data, are several times greater than for other harmonics.

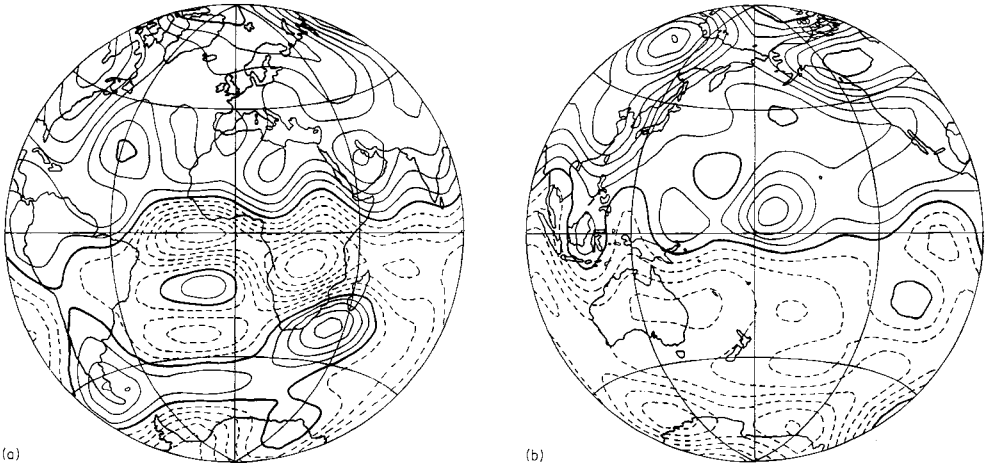

Figure 2. Contour map of the radial field at the CMB for model D80111, epoch 1980. Contour interval is 100 μT; solid contours represent flux into the core, dashed contours flux out of the core. The thicker lines are null-flux curves. The projection is Lambert equal area.

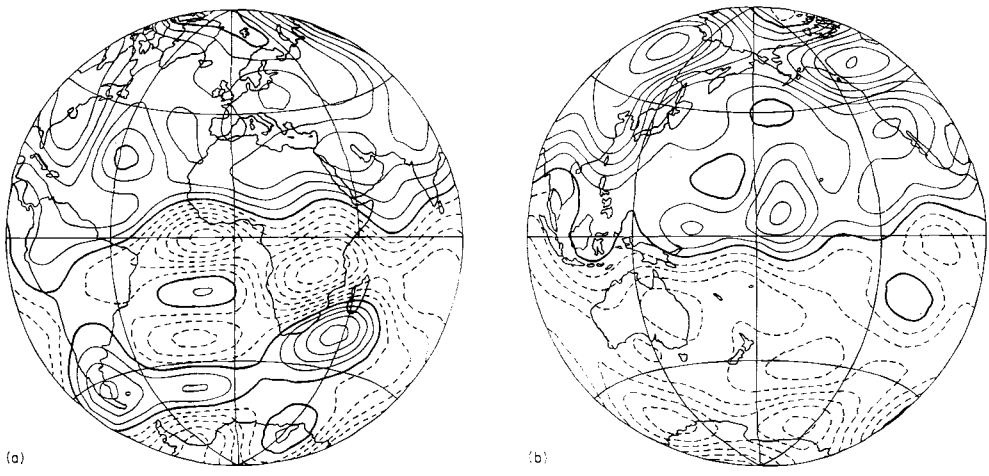

Figure 3. Contour map of the radial field at the CMB for model D69111, epoch 1969.5.

Equation (30) gives weaker prior information and the error estimates are correspondingly greater. Models were produced for 1980 for a variety of damping constants. The models were virtually indistinguishable from those derived from (34). The error estimates were larger, however, A model with $\lambda = 5 \times 10^{-11}$ had misfit $\sigma = 1.07$, remainder error of 44 μT and a total error of about 60 μT. The errors in the very high-degree terms dominate with this choice of prior information. All other models reported on in this paper were calculated using (34).

4.2 THE EFFECT OF VARYING THE DAMPING CONSTANT

Choosing a large value of the damping constant produces a smooth core field and small variance. A small value of the damping constant produces a rough model but many of the

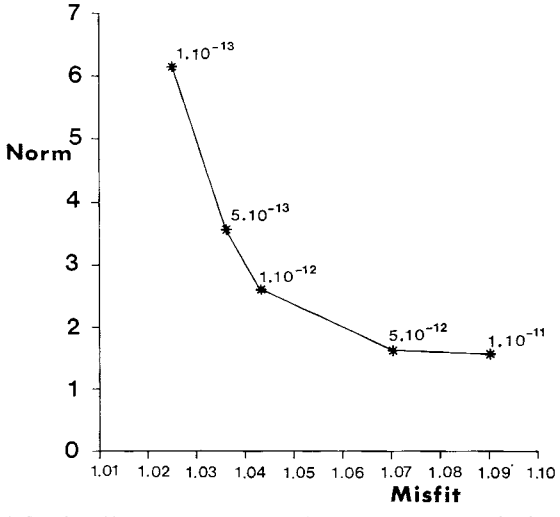

Figure 4. Trade-off curve for the 1980 field models. Dimensionless units.

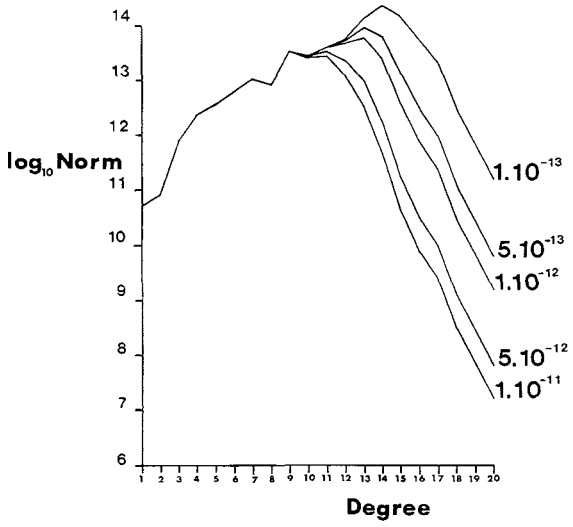

Figure 5. Model norm by spherical harmonic degree for 1980 field models.

details may be submerged in the larger noise. We regard all solutions as valid when taken with their error estimates: any interpretation should not depend on the model used, provided our prior information is not too strong.

The trade-off curve for the 1980 models is shown in Fig. 4. The model in Fig. 2 has $\lambda = 10^{-11}$ and corresponds to the smooth, heavily damped end of the trade-off curve. Fig. 5 shows the contribution to the norm $\mathbf{m}^T \mathbf{C}_m^{-1} \mathbf{m}$, by spherical harmonic degree, for the 1980 models. The dramatic drop in the contribution occurs when prior information dominates, which is at a higher degree for smaller values of λ. Resolution, as given by the diagonal elements of the resolution matrix, is plotted in Fig. 6. Resolution is very good for the low-degree coefficients, and again it falls off dramatically when the prior information takes over. The fall-off occurs at higher degree for a smaller damping constant.

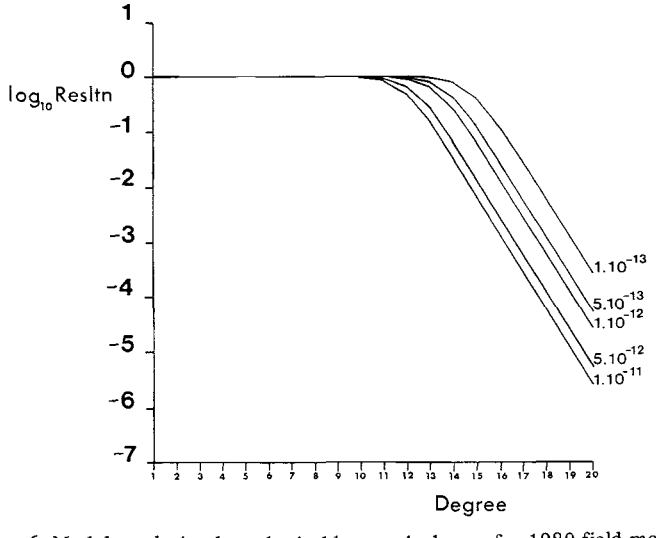

Figure 6. Model resolution by spherical harmonic degree for 1980 field models.

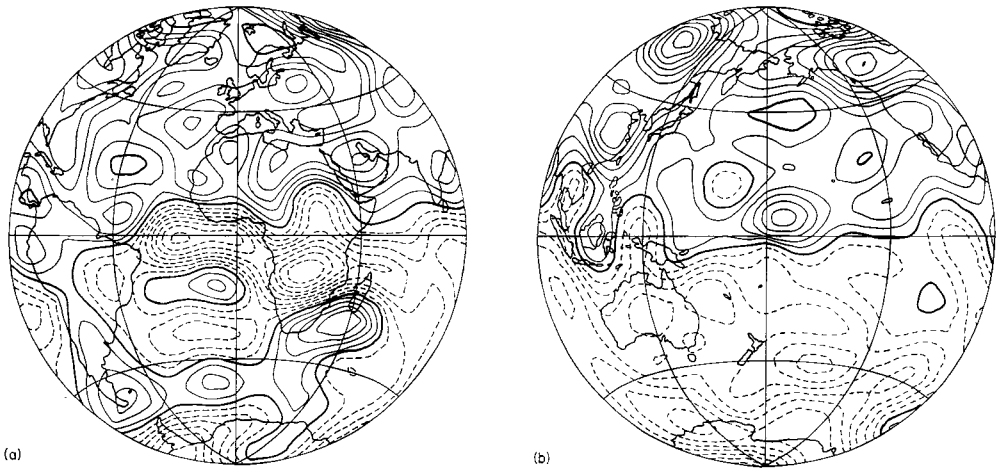

Figure 7. Contour map of the radial field at the CMB for model D80513, epoch 1980.

4.3 ROUGHER CORE FIELDS

The trade-off curves suggest we try smaller values of the damping constant. Two more models are shown in Figs 7 and 8. Fig. 7 has a 1980 model with $\lambda = 5 \times 10^{-13}$, $\sigma = 1.04$; Fig. 8 has a 1969.5 model with $\lambda = 5 \times 10^{-13}$ and $\sigma = 1.27$. The errors for the 1980 model are about 106 μT. The traces for the resolution matrices are 203 and 197 respectively.

In comparing Figs 7 and 8 we see some very similar features. The topologies of the null flux curves are the same except for some features in the Pacific. These differences are well within the errors. The undulations in the magnetic equator under Indonesia are present in both plots but are more intense in 1980 – probably a real change. The models are based on totally different datasets, collected 10 yr apart, one being mainly total field data and the other vector data. Their similarity is further indirect evidence that these features can be believed, and that our error estimates are realistic.

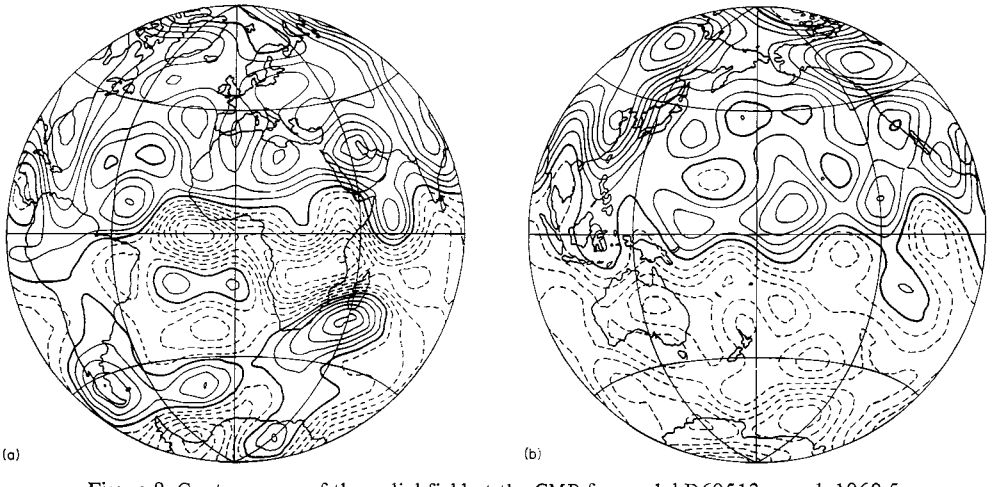

Figure 8. Contour map of the radial field at the CMB for model D69513, epoch 1969.5.

5 Conclusions

5.1 THE CORE FIELD

The major conclusion of this paper is that the core field is much more complex, and contains far more short-wavelength field, than has hitherto been supposed. The maps displayed in Figs 2 and 3 show very much more detail than appears on a map of, for example, the 1965 IGRF or DGRF, and yet our error analysis shows that most of these features are real. The method does not discriminate between true core field and long-wavelength crustal anomalies. Any crustal field will be mapped into an apparent core field.

Null-flux curves, where $B_r = 0$ on the CMB, play an important role in the frozen-flux theory of secular variation. Core fields based on truncated spherical harmonic series all give similar pictures for the null-flux curves, regardless of epoch, with a magnetic equator, one under South America, one under South Africa, and two other small curves in the North Pacific and Arctic (Shure *et al.* 1983, fig. 1). The fields presented in this paper are quite different. The null-flux curves for the 1980 model are shown in Fig. 9, together with the error corridor for one standard deviation. The magnetic equator now has sharp bends under Indonesia, there is one large null-flux curve in the South Atlantic and a second, smaller one to the north. There are four more small curves, most of which appear to be significant. These curves are also apparent in conventional *Magsat* models with high truncation, but they have previously been believed to be spurious (Benton *et al.* 1982). The new configuration of null-flux curves will radically alter the core motions determined using the frozen-flux approximation.

5.2 SECULAR VARIATION

Secular variation was estimated from the difference between models D80111 and D69111 (Figs 2 and 3) and dividing by 10.5 yr. The result is a spherical harmonic model with similar low-degree coefficients to those reported in papers I and II, but the high-degree coefficients are very much larger. The resulting map is very rough in appearance, indicating very much weaker damping than was used in the earlier secular variation calculations.

The distribution of observatories is similar for both the new MF models and the earlier secular variation models. The process of using 1980 measurements to correct for the crustal

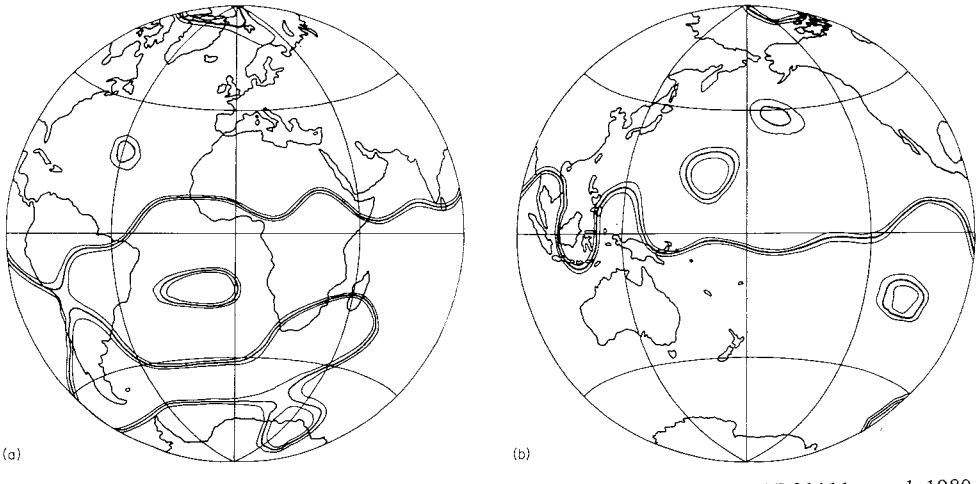

Figure 9. One standard deviation error bounds on the null-flux contours for model D80111, epoch 1980.

fields means that we are effectively using the observatories of categories A and B to define field differences between 1969.5 and 1980; in other words secular variation. We should therefore expect the data quality for the MF models to be as good as, if not better than, that for secular variation, because it includes additional satellite data. Error estimates on the fields suggest an error on their differences of about 4000 nT yr^{-1}, not much less than the maximum SV reported in paper I. It is not surprising, therefore, that the secular variation map appears rough.

The noise can be reduced by increasing the damping constant. This is the usual procedure, and it was followed in papers I and II, but it is not strictly honest. Prior information is obtained without recourse to the measurements, and should therefore be completely independent of them. Increasing the damping will produce a perfectly acceptable model, but the error estimates will be too small because our prior information is too strong, leading in this case to unjustifiably small error estimates in the degree range 6–13, for which the data lack resolving power but which are too large in scale for the prior information to apply.

There is some evidence that the damping used in papers I and II was too heavy. The flux integral over the northern hemisphere indicated a fall in magnitude several times larger than the standard deviation, mainly due to the decay of the dipole term. This had been noticed earlier by Booker (1969). The new field models have rather different null-flux curves, but this difference does not affect the integral significantly. To this extent the assumption, that the errors in the MF model could be neglected, is justified.

The corresponding flux integral for models D80111 and D69111 are 17.544 and 17.478 GWb respectively, an increase of 7 MWb yr^{-1}, in contradiction to the previous results which showed a decrease of 9 MWb yr^{-1}. Furthermore the change in the magnetic equator between 1969 and 1980 is so great that the dipole term alone causes an increasing contribution to the integral. The error estimate on each integral is about 30 MWb, however, showing that these differences are not significant. We have therefore answered the question raised by Booker (1969): the new data are sufficiently good to resolve the high harmonics and show that the observed decay of the dipole is consistent with the frozen-flux hypothesis. It also indicates that the error analysis of papers I and II was optimistic.

There remains the fundamental difficulty that our prior information is still too strong even for the *Magsat* data. We can only address this problem by making better measurements and achieving a better understanding of the core processes. If we do make the damping weaker then the field model will be so rough that the frozen-flux approximation will be invalidated: already model D80111 gives a dissipation integral in (33) that is 23 per cent of the secular variation term on the left side of (32), based on the secular variation models of paper I.

Acknowledgments

We thank Dr R. A. Langel for his helpful advice and, with Dr R. Estes, for supplying us with *Magsat* and POGO data. This work was partially supported by Natural Environment Research Council Grant GR3/3475. JB is supported by a NERC studentship.

References

Backus, G. E., 1970. Non-uniqueness of the external geomagnetic field determined by surface intensity measurements, *J. geophys. Res.*, **75**, 6339–6341.

Bard, Y., 1974. *Non-linear Parameter Estimation*, Academic Press, New York.

Barraclough, D. R. & Nevitt, C. E., 1976. The effect of observational errors on geomagnetic field models based solely on total-intensity measurements, *Phys. Earth planet. Int.*, **13**, 123–131.

Benkova, N. P., Dologinov, S. S., Tyurmina, L. O. & Cherevko, T. N., 1971. Comparison between the two satellite models, Izmiran and Pogo, in *World Magnetic Survey, 1967–1969*, ed. Zmuda, A. J., *Bull. int. Ass. Geomagn. Aeron., Paris*, **28**, 158–163.

Benton, E. R., Estes, R. H., Langel, R. A. & Muth, L. A., 1982. Sensitivity of selected geomagnetic properties of truncation level of spherical harmonic expansions, *Geophys. Res. Lett.*, **9**, 254–257.

Booker, J. R., 1969. Geomagnetic data and core motions, *Proc. R. Soc. A*, **309**, 27–40.

Box, G. E. P. & Tiao, G. C., 1973. *Bayesian Inference in Statistical Analysis*, Addison-Wesley, London.

Gubbins, D., 1975. Can the earth's magnetic field be sustained by core oscillations?, *Geophys. Res. Lett.*, **2**, 409–412.

Gubbins, D., 1983. Geomagnetic field analysis – I. Stochastic inversion, *Geophys. J. R. astr. Soc.*, **73**, 641–652.

Gubbins, D., 1984. Geomagnetic field analysis – II. Secular variation consistent with a perfectly conducting core, *Geophys. J. R. astr. Soc.*, **77**, 753–766.

Gubbins, D. & Roberts, N., 1983. Use of the frozen-flux approximation in the interpretation of archaeomagnetic and palaeomagnetic data, *Geophys. J. R. astr. Soc.*, **73**, 675–687.

Hurwitz, L. & Knapp, D. G., 1974. Inherent vector discrepancies in geomagnetic main field models based on scalar *F*, *J. geophys. Res.*, **79**, 3009–3013.

Jackson, D. D., 1979. The use of *a priori* data to resolve non-uniqueness in linear inversion, *Geophys. J. R. astr. Soc.*, **57**, 137–157.

Langel, R. A., Coles, R. L. & Mayhew, M. A., 1980. Comparison of magnetic anomalies of lithospheric origin measured by satellite and airborne magnetometers over Western Canada, *Can. J. Earth Sci.*, **17**, 876–887.

Langel, R. A. & Estes, R. H., 1984. The near Earth magnetic field at 1980 determined from *Magsat* data, *J. geophys. Res.*, to appear.

Langel, R. A., Estes, R. H. & Mead, G. D., 1982. Some new methods in geomagnetic field modelling applied to the 1960–1980 epoch. *J. Geomagn. Geoelect.*, **34**, 327–349.

Lowes, F. J., 1975. Vector errors in spherical harmonic analysis of scalar data, *Geophys. J. R. astr. Soc.*, **42**, 637–651.

Luenberger, D. G., 1969. *Optimization by Vector Space Methods*, Wiley, New York.

Shure, L., Parker, R. L. & Backus, G. E., 1982. Harmonic splines for geomagnetic modelling, *Phys. Earth planet. Int.*, **28**, 215–229.

Shure, L., Whaler, K., Gubbins, D. & Hobbs, B., 1983. Physical constraints for the analysis of the geomagnetic secular variation, *Phys. Earth planet. Int.*, **32**, 114–131.

Stern, D. P. & Bredekamp, J. H., 1975. Error enhancement in geomagnetic models derived from scalar data, *J. geophys. Res.*, **80**, 1776–1782.

Stern, D. P., Langel, R. A. & Mead, G. D., 1980. Backus effect observed by *Magsat*, *Geophys. Res. Lett.*, **7**, 941–944.

Tarantola, A. & Valette, B., 1982. Generalized non-linear inverse problems solved using the least squares criterion, *Rev. Geophys. Space Phys.*, **20**(2), 219–232.

Theil, H., 1963. On the use of incomplete prior information in regression analysis, *J. Am. statist. Ass.*, **58**, 401–414.

Toutenburg, H., 1982. *Prior Information in Linear Models*, Wiley, Chichester.

Appendix: Analysis of total intensity data

Following the launch of the *OGO-2* satellite in 1965 into a polar orbit, accurate, globally distributed observations of the magnetic field became available for the first time. The *OGO* generation of satellites observed only the total field intensity, F; from these observations many models of the field have been produced using non-linear least-squares methods. However, it was soon recognized that models based entirely on these data contained large discrepancies in the components of the magnetic field vector, although having a good fit to the intensity data: moreover, these discrepancies followed a regular pattern (Benkova *et al.* 1971) with, in particular, the largest discrepancies occurring in the radial component of the field in the vicinity of the magnetic equator.

Contemporaneously, Backus (1970) showed, by exhibiting a specific counter-example, that the magnetic scalar potential is not necessarily determined uniquely from the knowledge of the field intensity everywhere on the surface $r = a$. Stern & Bredekamp (1974)

proposed that the discrepancies may be related to the form of the counter-example exhibited by Backus; Stern, Langel & Mead (1980) have produced some evidence in favour of this proposition.

Lowes (1975) offered a particularly simple explanation of these discrepancies in terms of the perpendicular error effect: the tendency for the error vector to be perpendicular to the true vector. This explanation is consistent with the observation that the discrepancies in the radial field follow the magnetic equator very closely. In either case the effect on a spherical harmonic series is the same: it is the vectorial harmonics that are poorly determined by total intensity data.

The requirement, as part of the main study described in this paper, to produce a field model for 1969.5 (when the only satellite data available were total intensity data) motivated a re-examination of suggestions which have been made for reducing the effect. Hurwitz & Knapp (1974) suggested the use of some 3-component ('vector') data and Barraclough & Nevitt (1976) conclude that approximately 10 per cent of vector data is required.

Data, with added Gaussian noise, were synthesized from an IGRF model in order to investigate these suggestions further. F data were synthesized at a grid of points with an approximately even distribution in area, and vector data at a selection of observatory sites. Models were produced using varying proportions of these two sets of data and compared with the original model. The results were quite straightforward: adding vector data greatly improves the determination of the sectorial harmonics and so reduces the discrepancies in the computed radial field. However, the amount of vector data which is required is not dependent on the amount of F data used: adding more F data serves to improve further the resultant model. There is no limit placed on the amount of F data which may be used by the availability of vector data.

It is useful to remember that these discrepancies are reflected in the covariance matrix of the estimates and so, by examination of the covariance matrix, it is possible to check whether a particular model suffers significantly from this effect.